Numerical schemes for a pseudo-parabolic Burgers equation : discontinuous data and long-time behaviour

Numerical schemes for a pseudo-parabolic Burgers equation: discontinuous data and long-time behaviour

C. M. Cuesta*, I. S. Pop†

Abstract

We consider a simplified model for vertical non-stationary groundwater flow, which includes dynamic capillary pressure effects. Specifically, we consider a viscous Burgers'–type equation that is extended with a third-order term containing mixed derivatives in space and time. We analyse the one–dimensional boundary value problem and investigate numerically its long time behaviour. The numerical schemes discussed here take into account possible discontinuities of the solution.

Keywords: pseudo-parabolic equations, Burgers equation, numerical schemes at interfaces, long-time behaviour.
2000 Mathematics Subject Classification: 35M99, 35B40, 35B65, 65N30, 65N15

1 Introduction

In this paper we present a numerical method to approximate the Cauchy problem

$$u_t = u_{xx} + (u^2)_x + \varepsilon\, u_{xxt} \quad \text{on} \quad \mathbb{R}\times\mathbb{R}^+,\ \varepsilon > 0\,, \tag{1.1}$$

$$u(x,0) = u_0(x) \quad \text{in} \quad \mathbb{R}\,. \tag{1.2}$$

The numerical method is designed to accuratelly deal with discontinuous data. A second aim of this paper is to illustrate the long-time behaviour of solutions: equation (1.1) reduces to a viscous Burgers equation when $\varepsilon = 0$, cf. [13]. As $t \to \infty$, solutions of Burgers equation converge either to a self-similar source type solution, or to a rarefaction wave, or to a travelling wave solution. The type of the limiting solution depends on whether the initial data u_0 satisfies $u_0(-\infty) = u_0(+\infty)$, $u_0(-\infty) < u_0(+\infty)$ or $u_0(-\infty) > u_0(+\infty)$, see [14] and [13]. A similar type of behaviour can be expected for the solution of (1.1), at least for small values of ε.

We investigate numerically the initial value problem

$$u_t = u_{xx} + (u^2)_x + \varepsilon u_{xxt} \quad \text{on } (-l,l)\times[0,T], \tag{1.3}$$

with an initial condition satisfying

$$u_0(-l) = u^-,\ u_0(l) = u^+\,, \tag{1.4}$$

we also impose boundary conditions on $w := u + \varepsilon u_t$:

$$w(-l,t) = u^- \quad w(l,t) = u^+ \quad \text{for } t \in (0,T). \tag{1.5}$$

*School of Mathematical Sciences, Theoretical Mechanics, University of Nottingham, University Park, NG7 2RD, Nottingham, UK, E-mail: carlota.cuesta@maths.nottingham.ac.uk
†Department of Mathematics and Computer Science, Eindhoven University Technology P.O. Box 513, 5600 MB Eindhoven, The Netherlands, E-mail: ipop@win.tue.nl

Here u^- and u^+ are non-negative constants. And $l > 0$ is taken sufficiently large in the numerical examples as to get a reasonable approximation of (1.1).

Equation (1.1) is motivated by the degenerate pseudo-parabolic equation

$$u_t = \{u^\alpha + u^\beta u_x + u^\alpha (u^\gamma u_t)_x\}_x \,, \tag{1.6}$$

for α, β and $\gamma > 0$. Equation (1.6) was considered in [7] as a model of one-dimensional unsaturated groundwater flow. Here u denotes the water saturation. Equation (1.6) follows by combining Darcy's law, the mass conservation equation for the water phase, and an interfacial relation, given by a capillary pressure relation. We refer to [3] for a detailed explanation of the model. Notice that equation (1.6) differs from the classical convective porous medium equation (see [4]) in the mixed derivatives third order term (with derivatives in space and time). This term appears as a result of considering a *dynamic* capillary pressure relation instead of a usual static one (cf. [10]). In the simplest formulation, the extended pressure relation reads

$$p_a - p_w = p_c(u) + \varepsilon L u_t. \tag{1.7}$$

Where p_a stands for the (constant) air pressure, p_w is the water pressure, while $p_c(u)$ is the capillary pressure function. The factor L is a damping coefficient that may depend on u, and ε is a positive constant introduced as a control parameter ($\varepsilon = 0$ is the static pressure case).

Existence of global travelling wave solutions separating wet and dry regions is studied in [7]. These solutions are postulated to describe the long-time behaviour of solutions for initially almost dry regions. Many question remain open for (1.6). The main difficulty comes from the degenerate diffusion term in combination with the mixed derivatives one. Regularisation techniques on positive data, as for PME, cannot be applied, due to the lack of maximum and comparison principles. A rigorous proof of stability of travelling waves remains open. In this respect equation (1.1) is considered to be the simplest pseudo-parabolic equation allowing travelling wave solutions. Indeed, (1.1) subject to initial data u_0 satisfying $u_0(-\infty) = 0 < u_0(+\infty) = 1$ is investigated in [6], where stability of monotone travelling waves is proved. Stability of the non-monotone ones, has not yet been rigorously proved. We recall that monotonicity of travelling waves depends on ε, $\varepsilon \leq \frac{1}{4}$ being a sufficient condition for monotonicity. In [8], linear stability analysis of travelling wave solutions is studied via numerical examination of the Evans function. This analysis suggests that non-monotone travelling waves are stable too. Further evidence comes from the numerical examples that follow. We shall as well show numerical examples suggesting convergence to the other possible asymtotic solutions.

Two numerical schemes are used: a first order explicit in time and a implicit in time one. Spatial discretization is achieved by first order upwind schemes, see [16]. In conservative form, equation (1.3) reads

$$u_t = F_x \,, \tag{1.8}$$

with the flux $F = u^2 + w_x$, while the *pressure* w satisfies the elliptic equation

$$-\varepsilon w_{xx} + w = u + \varepsilon (u^2)_x \,. \tag{1.9}$$

The first two equations are solved alternatively for the explicit discretization, while in the implicit case we solve (1.9) and $\varepsilon u_t = w - u$ simultaneously.

The conservation form in (1.8) brings some advantages in case of discontinuous initial data. As shown in [6], if u_0 has a jump discontinuity at some $x_0 \in \mathbb{R}$, then so does the solution for every $t \geq 0$. By mass conservation, the flux is continuous at the jump location, moreover one can show that w is continuous too. These properties will be use as continuity conditions across the solution jumps. Similar approaches can be found in [20] or [22], where interface conditions between different homogeneous porous layers are imposed.

Numerical methods for similar equations are considered, for example, in [5] and [9], where the finite elements method (FEM) is used. These papers are motivated by the so-called Benjamin-Bona-Mahony-Burgers (BBM-B) equation that arises in the context of long wave motion, see [5] for a derivation of the model. The analysis carried out in these works results in error estimates, but no jump discontinuities are considered. We also mention the work [11], where a numerical treatment of an unsaturated flow model with a dynamic capillary pressure relation also accounting for hysteresis is performed. No convection driving term is present however.

We mention that (1.1) can be seen as a regularisation (by higher order terms) of the (inviscid) Burgers equation. In this context, (1.1) is closely related to the KdV-Burgers equation: for scalar conservation laws with a non-convex flux, both regularisations lead to *non-classical* shocks, see [15] and [21]. Most recently, a numerical investigation of a Buckley-Leverett equation extended with dynamic capillary pressure effects in a hererogeneous medium has been considered in [12].

This paper is organised as follows. In Section 2 we indicate the main qualitative properties of solutions to problem (1.3)-(1.5) upon which the numerical methods are constructed.

Section 3 describes the numerical schemes, including the treatment of jump discontinuities. For the implicit scheme we apply an iterative semi-implicit scheme, which is shown to converge in Appendix A.

In Section4 we give numerical examples. We observe that the long-time behaviour of the (viscous and inviscid) Burgers equation and of (1.3) is similar. More specifically, if the initial data satisfies $u^- < u^+$, the solution converges to a travelling wave, while for an initial having $u^- > u^+$ the solution should rather approximate a rarefaction wave profile as $t \to \infty$. Finally, if $u^+ = u^-$, the expected limiting profiles are approximations of N-waves, or rather approach the self-similar solution of the viscous Burgers equation. The numerical examples sustaining these predictions are given in this section. Also, at the end of the section we give it numerical examples for small times to illustrate the evolution of jump discontinuities in the initial data. In particular, when $u^- \geq u_0 \geq u^+ = 0$ with ε large enough, the numerical solutions become non-positive at early time steps.

Throughout the paper $\|\cdot\|$ denotes the L^2-norm with the usual inner product denote by $(\cdot,\cdot)$, $\|\cdot\|_1$ stands for the H^1-norm and $\|\cdot\|_\infty$ for the L^∞-norm. We also introduce the following coercive ($\varepsilon > 0$) bilinear form in H^1,

$$a_\varepsilon(u, v) := (u, v) + \varepsilon(u_x, v_x),$$

and denote the associated norm by $\|\cdot\|_\varepsilon$. This norm is equivalent to $\|\cdot\|_1$:

$$\|u\|_\varepsilon \leq C_\varepsilon \|u\|, \quad \|u\| \leq c_\varepsilon \|u\|_\varepsilon, \tag{1.10}$$

where $C_\varepsilon = 1$ and $c_\varepsilon = \frac{1}{\varepsilon}$ if $\varepsilon \leq 1$, respectively $C_\varepsilon = \varepsilon$ and $c_\varepsilon = 1$ if $\varepsilon > 1$.

Finally, we mention that a combination of integral estimates, as in [6], and Fourier transform techniques are used in a number of papers dedicated to long-time behaviour of the Cauchy problem for BBM-Burgers' equation when a source type initial data is considered, see for instance [1] and references therein.

2 Analytical results

In this section we give some analytical results that are analogous to those proved in [6]: well-posedness, persistence in time of jump discontinuities, conservation of mass, and global existence of solutions.

To prove well-posedness, problem (1.3)-(1.5) is formulated by introducing the unknown $w = u + \varepsilon u_t$. Formally, w satisfies the elliptic equation (1.9) with boundary conditions $w(-l) = u^-$ and $w(l) = u^+$. Note that since u itself is time dependent, t appears as a parameter in (1.9).

To define w rigorously we use the non-linear operator

$$w := W(u) + \bar{w} = G_\varepsilon \left(u + \varepsilon (u^2)_x\right) + \bar{w}. \tag{2.1}$$

Where G_ε is the Green's function associated to the operator $(I - \varepsilon \frac{d^2}{dx^2})^{-1}$ on $(-l, l)$ solving for a w such that $w(\pm l) = 0$. While $\bar{w}$ is a solution of $-\varepsilon w_{xx} + w = 0$ in $(-l, l)$ with boundary conditions $\bar{w}(\pm l) = u^\pm$. We reformulate (1.3)-(1.5) as the following 'initial value' problem

$$u_t = \frac{1}{\varepsilon}\left(W(u) - u\right) + \frac{1}{\varepsilon}\bar{w}, \quad \text{on } (-l, l) \times [0, T] \tag{2.2}$$

$$u(\cdot, 0) = u_0(\cdot) \quad \text{in } (-l, l), \quad \text{and } u_0(\pm l) = u^\pm. \tag{2.3}$$

Theorem 2.1 *Let $X = L^2(-l, l)$, or $H^1(-l, l)$. If $u_0 \in X$, a $T > 0$ exists so that problem (2.2)–(2.3) has a unique solution $u \in C^1(0, T; X)$.*

Proof. The proof follows the ideas in [6] for the Cauchy problem on $\mathbb{R}$. The operator $\mathcal{L}(u) = \frac{1}{\varepsilon}(W(u) - u)$ maps X to X, and is locally Lipschitz continuous. Then by Picard's theorem for ordinary differential equations in Banach spaces, equation (2.2) has a unique solution in $C^1(0, T; X)$. □

The next lemma shows that the solution has the same boundary values as the initial condition, and also deals with the evolution on t of discontinuities of the initial condition. The proof uses the variation of constants formula applied to (2.2), i.e.

$$u(\cdot, t) = u_0(\cdot) \exp\left(\frac{-t}{\varepsilon}\right) + \frac{1}{\varepsilon}\int_0^t w(\cdot, s) \exp\left(\frac{-(t-s)}{\varepsilon}\right) ds \quad \text{for } t \in [0, T], \tag{2.4}$$

with w given by (2.1).

Lemma 2.2 *Let u_0 in $L^2(-l, l)$, then*

(i) If u_0 has a jump discontinuity at x_0, then so does the corresponding unique solution u. Moreover the jump decreases according to

$$u(x_0^-,t) - u(x_0^+,t) = \exp\left(\frac{-t}{\varepsilon}\right)(u_0(x_0^-) - u_0(x_0^+)) \quad \textit{for all } t \in [0,T], \quad (2.5)$$

where $u(x_0^+)$ ($u(x_0^-)$) denotes the left (right) limit of u at x_0.

(ii) If $\lim_{x\to -l} u_0(x) = u^-$ and $\lim_{x\to +l} u_0(x) = u^+$ exist, then the solution u of (2.2) also satisfies

$$u(-l,t) = u^- \quad \textit{and} \quad u(l,t) = u^+ \quad \textit{for } t \in [0,T]\,.$$

Proof. *(i)* As in [6], one can see that G_ε is a continuous operator from $L^2(-l,l)$ to $H^1(-l,l)$, i.e. $w \in H^1(-l,l)$. This together with (2.4) imply the estatement.
(ii) Let $\delta > 0$ be small enough such that u_0 is continuous on $(-l,-l+\delta)$ and on $(l-\delta,l)$. By *(i)*, u is continuous on these intervals as well, so the limits $x \searrow -l$ and $x \nearrow l$ in (2.4) are well-defined, and we can take the limits $x \to \pm l$ in (2.4). □

Remark 2.3 *Lemma 2.2-(i) can be extended to the case of initial conditions with multiple jump discontinuities, like $u_0 = v_0 + \sum_{i=0}^N C_i H_{x_i}$, with $v_0 \in C([-l,l])$, and $C_i \in \mathbb{R}$ for all $i = 0 \dots N$. Here H_{x_i} denotes a Heaviside graph with the jump at x_i.*

As for the diffusive Burgers equation, mass is conserved for (1.1) (see [6]). The analogous property holds (2.2)-(2.3):

Proposition 2.4 *If $u_0 \in L^2(-l,l)$, then the flux $F = w_x + u^2$ is continuous. Moreover, the solution u of (2.2)-(2.3) satisfies*

$$\int_{-l}^{l} u(x,t)dx = \int_{-l}^{l} u_0(x)dx - \int_0^t (F(-l,s) - F(l,s))ds \quad \textit{for } t \in [0,T]. \quad (2.6)$$

Proof. We first notice that by (2.1) and (2.2) the flux F defined in (1.8) satisfies

$$F_x = w_{xx} + (u^2)_x = (w-u)/\varepsilon \quad (2.7)$$

in the sense of distributions. By Theorem 2.1, $u \in C^1(0,T;L^2(-l,l))$ and then also $w \in C(0,T;L^2(-l,l))$. It now follows from (2.7) that $F_x \in C(0,T;L^2(-l,l))$. By definition, $F \in C(0,T;L^2(-l,l))$, thus $F \in C(0,T;H^1(-l,l))$, implying the continuity.

The proof of (2.6) is standard: one can test (2.2) with a family of functions $\varphi_\tau \in C(-l,l)$ with $\varphi_\tau(\pm l) = 0$ and such that $\varphi_\tau \to 1$ as $\tau \searrow 0$ strongly in $L^2(-l,l)$. Passing to the limit $\tau \searrow 0$ involves no difficulty. □

The next proposition gives integral estimates for equation (1.3), which ensure global existence of solutions in $H^1(-l,l)$. We first need the following lemma

Lemma 2.5 *Assume that the boundary values $u^+, u^- \geq 0$, then there exists a unique stationary solution h of equation (1.3) such that $h(-l) = u^-$ and $h(l) = u^+$, and h is monotone in $[-l,l]$.*

Proof. A stationary solution h of (1.3) must satisfy

$$h' + h^2 = C, \quad \text{in } [-l, l], \tag{2.8}$$

with $C = h'(\pm l) + (u^{\pm})^2 \in \mathbb{R}$. The initial value problem to (2.8) with initial condition $h(-l) = u^-$ is well-posed for any $C \in \mathbb{R}$. Moreover, if $C \geq 0$, h is explicitly given by

$$h(x) = \frac{c(1 - e^{2(x+k)c})}{1 + e^{2(x+k)c}}$$

where

$$c = \sqrt{C}, \quad k = \frac{1}{2c} \ln \left(\frac{c - u^-}{c + u^-} \right) + l.$$

When $C < 0$, h is given by

$$h(x) = -c \tan((x + k)c) \quad \text{with} \quad c = \pm\sqrt{-C}, \quad k = \frac{1}{c} \arctan \left(-\frac{u^-}{c} \right) + l.$$

It is easy to see that the condition $u^+ = h(l)$ gives u^+ as a well defined function of C. The monotonicity of h follows by inspection of (2.8). □

Proposition 2.6 *Let $u^+, u^- \geq 0$ and $u_0 \in \{u \in H^1(-l, l) : \ u(-l) = u^-, u(l) = u^+\}$. Let h be the stationary solution of (1.3) such that $h(-l) = u^-$ and $h(l) = u^+$, then the solution u of (1.3) exists globally in t and satisfies*

(i) If $u^- \geq u^+$, then $t \to \|u(t) - h\|_\varepsilon^2$ decreases as $t \to \infty$.

(ii) If $u^- < u^+$, then

$$\|u(t) - h\|_\varepsilon^2 \leq \exp(Kt) \|u_0 - h\|_\varepsilon^2 \quad \text{for all } t \geq 0,$$

where $K = h'(-l) > 0$.

Proof. Using the weak formulation of (1.9), and equation (2.2), we get equation (1.3) in weak form as

$$\int_{-l}^{l} u_t \varphi \, dx + \varepsilon \int_{-l}^{l} u_{tx} \varphi_x \, dx = -\int_{-l}^{l} u_x \varphi_x \, dx - \int_{-l}^{l} u^2 \varphi_x \, dx \quad \text{for } \varphi \in H_0^1(-l, l). \tag{2.9}$$

Set $\tilde{u} := u - h$, then $\tilde{u} \in H_0^1(-l, l)$ and satisfies the equation

$$\int_{-l}^{l} \tilde{u}_t \varphi \, dx + \varepsilon \int_{-l}^{l} \tilde{u}_{xt} \varphi_x \, dx = -\int_{-l}^{l} \tilde{u}_x \varphi_x \, dx + \int_{-l}^{l} (\tilde{u}^2)_x \varphi \, dx + 2 \int_{-l}^{l} (\tilde{u}h)_x \varphi \, dx. \tag{2.10}$$

Setting $\varphi = \tilde{u}$ in (2.10) we get

$$\frac{1}{2} \frac{d}{dt} \int_{-l}^{l} (\tilde{u}^2 + \varepsilon \tilde{u}_x^2) \, dx = -\int_{-l}^{l} \tilde{u_x}^2 \, dx + \int_{-l}^{l} \tilde{u}^2 h' \, dx. \tag{2.11}$$

If $u^+ \geq u^-$, by Lemma 2.5, $h' \leq 0$. This with (2.11) imply *(i)*. For $u^- < u^+$, Lemma 2.5 gives $h'(x) \geq 0$. And *(ii)* is obtained by application of the Gronwall's lemma in (2.11). □

Remark 2.7 *Proposition 2.6 could be generalised to initial data with jump discontinuities, by using that the boundary terms that result at the jump locations decay exponentially with t. This is beyond the scope of this paper. Such a generalisation appears in [6] for the stability of monotone travelling waves.*

3 Numerical schemes

In this section we describe the numerical schemes used in Section 4 to approximate equation (1.3). We use the following notation: let $-l = x_0 < \ldots < x_{n+1} = l$ be a uniform partition of the spatial interval $I = [-l, l]$, with $h = x_{i+1} - x_i$. Also let $0 = t_0 < t_1 < \ldots < t_{m+1} = T$ be a uniform partition of the time interval $[0, T]$, and $\tau = t_{k+1} - t_k$.

The numerical approximations of u and w (solution of (1.3)- (1.9)) will be denoted by u^k and w^k at $t = k\tau$, respectively. Their values at a grid point x_i are denoted by u_i^k and w_i^k. For simplicity we consider discontinuous data with a single jump, located at the mid-point of the interval $[x_j, x_{j+1}]$ for some $j \in \{1, \ldots, n\}$. This point is denoted by $x_{j+\frac{1}{2}}$. By Lemma 2.2, the jump discontinuity will persist at $x_{j+\frac{1}{2}}$ as k increases. We add a left and right values of the numerical solution u^k at $x_{j+\frac{1}{2}}$: $u^{k,-}$ and $u^{k,+}$, respectively. Since w is continuous in space, only one additional value is needed for w^k at $x_{j+\frac{1}{2}}$: W^k. We next we describe the numerical schemes.

3.1 Explicit in time scheme

We use the eqution in conservation form (1.8)-(1.9). Knowing u^k at a given time step t_k, we first solve (1.9) numerically to obtain w^k. Next we use u^k and w^k in order to obtain u^{k+1} explicitly from (1.8).

To be more specific, we let u^k be given and, for simplicity, we assume that is positive, so that the flow takes place from the right only. On grid points, away from the discontinuity, we perform a first order left up-wind discretization of (1.9) at $t = t_k$, this reads

$$w_i^k - \frac{\varepsilon}{h^2}(w_{i-1}^k - 2w_i^k + w_{i+1}^k) = u_i^k + \frac{\varepsilon}{h}((u_{i+1}^k)^2 - (u_i^k)^2), \tag{3.1}$$

where $w_0^k = u^-$ and $w_{n+1}^k = u^+$. Next, u^{k+1} is given by

$$u_i^{k+1} - u_i^k = \frac{\tau}{h}(F_{i+\frac{1}{2}}^k - F_{i-\frac{1}{2}}^k), \quad \text{for } i = 0 \ldots n, \tag{3.2}$$

with the discrete up-wind flux

$$F_{i+\frac{1}{2}}^k := (u_{i+1}^k)^2 + \frac{1}{h}(w_{i+1}^k - w_i^k), \quad \text{for } i = 0 \ldots n.$$

The up-wind discretization is chosen because it satisfies the discrete version of (2.6) (as can be easily checked), i.e. this one-side discretization is conservative. In practice, the scheme adopted adapts the direction of the up-wind discretization to the sign of the numerical solution, i.e. right up-winding is performed at points where u^k is negative. The details are omitted for simplicity.

At the location of the jump $x_{i+\frac{1}{2}}$ we consider the left flux and the right flux

$$F_{j+\frac{1}{2}}^{k,-} = (u^{k,-})^2 + \frac{2}{h}(W^k - w_j^k),$$
$$F_{j+\frac{1}{2}}^{k,+} = (u_{j+1}^k)^2 + \frac{2}{h}(w_{j+1}^k - W^k).$$

We modify the discretization of (3.1) accordingly at the left and at the right of $x_{j+\frac{1}{2}}$:

$$w_j^k - \frac{\varepsilon}{h^2}(w_{j-1}^k - 2w_j^k + W^k) = u_j^k + \frac{\varepsilon}{2h}((u_{j+1}^k)^2 + (u^{k,-})^2 - 2(u_j^k)^2), \tag{3.3}$$

and

$$w_{j+1}^k - \frac{\varepsilon}{h^2}(W^k - 2w_{j+1}^k + w_{j+2}^k) = u_{j+1}^k + \frac{\varepsilon}{2h}(2(u_{j+2}^k)^2 - (u_{j+1}^k)^2 - (u^{k,-})^2). \tag{3.4}$$

The right hand sides in (3.3) and (3.4) result from the up-wind strategy. For example, $(u^2)_x$ is approximated in (3.3) by $(((u_{j+1}^k)^2 + (u^{k,-})^2)/2 - (u_j^k)^2)/h$. In this way at the jump discontinuity we take into account the contribution of u from both sides.

Now we determine W^k by imposing flux continuity at $x_{j+1/2}$, i.e. $F_{j+\frac{1}{2}}^{k,-} = F_{j+\frac{1}{2}}^{k,+}$, to obtain

$$W^k = \frac{h}{4}\left((u_{j+1}^k)^2 + \frac{2}{h}(w_{j+1}^k + w_j^k) - (u^{k,-})^2\right). \tag{3.5}$$

To get u^{k+1} away from the discontinuity we use (3.2), while at x_j and x_{j+1} we solve

$$u_j^{k+1} - u_j^k = \frac{\tau}{h}(F_{j+\frac{1}{2}}^{k,-} - F_{j-\frac{1}{2}}^k),$$
$$u_{j+1}^{k+1} - u_{j+1}^k = \frac{\tau}{h}(F_{j+\frac{3}{2}}^k - F_{j+\frac{1}{2}}^{k,+}).$$

Finally, we determine $u^{k+1,\pm}$, the values of u at the discontinuity by using the definition of w:

$$u^{k+1,\pm} = u^{k,\pm} + \frac{\tau}{\varepsilon}(W^k - u^{k,\pm}).$$

Observe that, if u is positive at the interface, $u^{k,+}$ is not used in the above approach. This is due to the right up-wind discretization. The case when u is negative is handled similarly.

3.2 Implicit in time scheme

The implicit scheme is based on the formulation of (1.3) given by equations (1.9) and (2.2). As before, we describe the scheme for positive u only, with the obvious changes at the points where u becomes negative. Assuming that u^{k-1} and w^{k-1} are given, at grid points not adjacent to the jump location the fully discrete equations read

$$w_i^k - \frac{\varepsilon}{h^2}(w_{i-1}^k - 2w_i^k + w_{i+1}^k) = u_i^k + \frac{\varepsilon}{h}((u_{i+1}^k)^2 - (u_i^k)^2), \tag{3.6}$$

and

$$u_i^k - u_i^{k-1} = \frac{\tau}{\varepsilon}(w_i^k - u_i^k). \tag{3.7}$$

The above scheme is nonlinear. We approximate it by iteration of a linear scheme. A straightforward semi-implicit linearization of (3.6) reads

$$w_i^k - \frac{\varepsilon}{h^2}(w_{i-1}^k - 2w_i^k + w_{i+1}^k) = u_i^k + \frac{\varepsilon}{h}(u_{i+1}^{k-1}u_{i+1}^k - u_i^{k-1}u_i^k), \tag{3.8}$$

which leads us to the iterative scheme

$$\begin{aligned} w_i^{k,s} - \tfrac{\varepsilon}{h^2}(w_{i-1}^{k,s} - 2w_i^{k,s} + w_{i+1}^{k,s}) &= u_i^{k,s} + \tfrac{\varepsilon}{h}(u_{i+1}^{k,s-1}\, u_{i+1}^{k,s} - u_i^{k,s-1}\, u_i^{k,s}), \\ u_i^{k,s} - u_i^{k-1} &= \tfrac{\tau}{\varepsilon}(w_i^{k,s} - u_i^{k,s}), \end{aligned} \tag{3.9}$$

where $s > 0$ is the iteration counter. Initially we take $u^{k,0} = u^{k-1}$ and $w^{k,0} = w^{k-1}$. Under some restrictions on the discretization parameters, convergence of $u^{k,s}$ to u^k (as $s \nearrow \infty$) is shown in Section A.4. Observe that now the flux function in (3.9) becomes

$$F_{j+\frac{1}{2}}^{k,s} := u_{j+1}^{k,s-1}\, u_{j+1}^{k,s} + \frac{1}{h}(w_{j+1}^{k,s} - w_j^{k,s}).$$

For grid points in the neighbourhood of the jump location we mention only those modifications that are specific to the semi-implicit discretization (3.8) – (3.7), iterations and fully implicit scheme being treated accordingly. At the left and right of $x_{j+\frac{1}{2}}$, (3.8) becomes

$$w_j^k - \frac{\varepsilon}{h^2}(w_{j-1}^k - 3w_j^k + 2W^k) = u_j^k + \frac{2\varepsilon}{h}(u^{k-1,-}\, u^{k,-} - u_{j+1}^{k-1}\, u_{j+1}^k), \tag{3.10}$$

and

$$w_{j+1}^k - \frac{\varepsilon}{h^2}(2W^k - 3w_{j+1}^k + w_{j+2}^k) - u_{j+1}^k - \frac{2\varepsilon}{h}(u_{j+2}^{k-1}u_{j+2}^k - u_{j+1}^{k-1}u_{j+1}^k) = 0, \tag{3.11}$$

respectively. The fluxes at the left and the right of a jump location are

$$\begin{aligned} F_{j+\frac{1}{2}}^{k,-} &= u^{k-1,-}\, u^{k,-} + \frac{2}{h}(W^k - w_j^k), \\ F_{j+\frac{1}{2}}^{k,+} &= u_{j+1}^{k-1}\, u_{j+1}^k + \frac{2}{h}(w_{j+1}^k - W^k). \end{aligned}$$

An equation for the pressure W^k follows again by imposing flux continuity, and reads

$$W^k = \frac{h}{4}\left(u_{j+1}^{k-1}\, u_{j+1}^k + \frac{2}{h}(w_{j+1}^k + w_j^k) - u^{k-1,-}\, u^{k,-}\right). \tag{3.12}$$

Finally, to determine $u^{k,\pm}$ we discretize (2.2) implicitly in t, this gives

$$\left(\frac{\tau+\varepsilon}{\varepsilon}\right) u^{k,\pm} - \frac{\tau}{\varepsilon} W^k = -u^{k-1,\pm}. \tag{3.13}$$

This way we end up with an algebraic system, that includes equations (3.8) for $i = 1 \ldots j-1$ and $i = j+2, \ldots, n$, to which we add (3.10), (3.11) and (3.12), and the equations (3.7) for $i = 1, \ldots, n$ and (3.13) for $u^{k,\pm}$.

4 Numerical examples

In this section we present numerical experiments that illustrate the long-time behaviour exhibited by solutions of (1.1). We begin with a heuristic explanation of the expected long-time, we also refer the reader to [23]. We end this section with examples illustrating the behaviour at jump discontinuities at early time steps.

There is no visual difference in the numerical solutions obtained by either the explicit or the implicit (iterative) discretization. Note that both methods have the same order of convergence, see Appendix A. The examples here are obtained with the explicit scheme.

4.1 Preliminaries

We first recall the large time behaviour for the inviscid Burgers equation and the diffusive (viscous) Burgers equation, from where we conclude formally the asymptotic behaviour for equation (4.1).

First we consider the scalar conservation law

$$u_t = (u^2)_x \quad \text{on } \mathbb{R}. \tag{4.1}$$

Observe that this equation is invariant under the group of scaling transformations $x \to \lambda x$ and $t \to \lambda t$, so that if $u(x,t)$ is a solution of (4.1), the family

$$u_\lambda(x,t) = u(x\lambda, t\lambda), \quad \text{for } \lambda \in \mathbb{R} \tag{4.2}$$

satisfies (4.1) as well. If one considers (4.1) subject to the Riemann condition

$$\begin{cases} u^+ & \text{if } x > 0 \\ u^- & \text{if } x \le 0, \end{cases} \tag{4.3}$$

it is well-known that for $1 = u^- > u^+ = 0$ the weak entropy solution is a *rarefaction wave* (a solution of the form $u(x,t) = f(\frac{x}{t})$), which is given by

$$r\left(\frac{x}{t}\right) := \begin{cases} 1 & \text{if } \frac{x}{t} \le -2 \\ -\frac{1}{2}\frac{x}{t} & \text{if } -2 \le \frac{x}{t} \le 0 \\ 0 & \text{if } \frac{x}{t} \ge 0. \end{cases} \tag{4.4}$$

Equation (4.1) is also invariant under translations in space and time. In fact if $0 = u^- < u^+ = 1$ in (4.3) then the weak entropy solution is a travelling shock wave, namely

$$g(x+t) = \begin{cases} 0 & \text{if } x + t < 0 \\ 1 & \text{if } x + t \ge 0. \end{cases} \tag{4.5}$$

Solutions of the Cauchy problem of (4.1) with bounded compactly supported initial data, tend to a so-called N-wave, see [17], a solution of (4.1). N-waves combine both travelling shock and rarefaction wave behaviour, in a way that mass is conserved. The graphs of this solutions are drawn in Figure 1 for completeness.

The diffusive (viscous) Burgers equation

$$u_t = u_{xx} + (u^2)_x \tag{4.6}$$

is invariant under the groups of transformations $x \to \mu x$, $t \to \mu^2 t$ and $u \to u/\mu$, and under translation in x and t. It is not invariant under the scaling (4.2). In fact the family u_λ satisfies the equation

$$u_{\lambda,t} = \frac{1}{\lambda} u_{\lambda,xx} + (u_\lambda^2)_x,$$

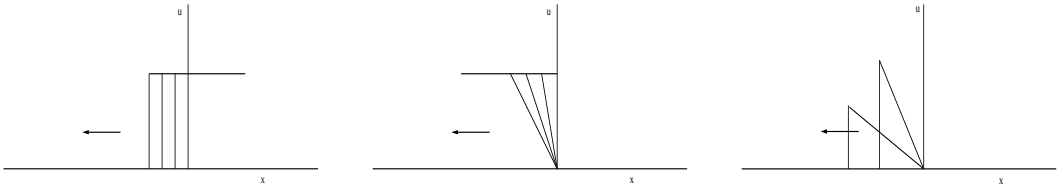

(a) Travelling shock. (b) Rarefaction. (c) N-wave.

Figure 1: Entropy solutions of (4.1)

that has (4.1) as limit equation for $\lambda \to \infty$. Similarly, the limit $\lambda \to \infty$ transforms to the limit $t \to \infty$, i.e for initial data such that $u^+ > u^-$ solutions tend to an approximation of a travelling shock that is a travelling wave solution of (4.6). This is consistent with the translation invariance of (4.6). For initial data with $u^+ < u^-$ solutions tend to an approximation of a rarefaction wave. Finally for initial data with $u^+ = u^- = 0$ solutions tend to an approximation of an N-wave, in this case a self-similar solution of equation (4.6), which is consistent with the invariance group of (4.6)

These results can be found in [14] and [13]. See also [23] for a more general theory on asymptotic behaviour of parabolic equations and conservation laws.

To apply the same argument to equation (1.1) we scale equation (1.1) according to (4.2). Then the family u_λ satisfies the equation

$$u_{\lambda,t} = \frac{1}{\lambda} u_{\lambda,xx} + (u_\lambda^2)_x + \frac{\varepsilon}{\lambda^2} u_{\lambda,xxt}.$$

Thus taking the limit $\lambda \to \infty$ we expect the limiting behaviour as $t \to \infty$ to be described by the formal *limit* equation (4.1). Then in the case $u^- < u^+$ travelling wave solutions are expected to describe the long time behaviour for any value of ε. In the other two cases we expect solutions to approximate rarefaction waves and N-waves respectively, as $t \to \infty$. In view of the third order term in the rescaled equation, we expect a slower convergence as ε gets larger, since for $\lambda < \varepsilon$ the third order term dominates.

4.2 Travelling waves

We take $u^+ = 1$ and $u^- = 0$, and the following step function as initial condition,

$$u_0(x) = \begin{cases} 1 & \text{if } x > 0 \\ 0 & \text{if } x \leq 0 \end{cases} . \tag{4.7}$$

Solutions are represented in the travelling wave coordinate $\eta = x + t$, with the wave speed $c = 1$, given by the Rankine Hugoniot condition $c = (u^+)^2 - (u^-)^2/(u^+ - u^-)$. Each graph in the figures corresponds to the profile at a time step. We have taken the half length of the interval to be $l = 100$. The step sizes are $h = 0.5$ and $\tau = 0.01$.

In Figure 4.2 we plot results for $\varepsilon = 0.2$ at time steps $t = 5, 10, 15$ and 20. In Figure 4.2 solutions are plotted for $\varepsilon = 5$, at time steps $t = 10, 15, 20, 25$ and 30. It is easily observed that the profiles tend to overlap (in the travelling coordinate)

as t increases, suggesting convergence to travelling waves. This convergence takes longer for $\varepsilon = 5$ than for $\varepsilon = 0.2$. Finally we observe that the profile of the solution oscillates when $\varepsilon = 5$, this being consistent with oscillatory travelling waves solutions found for $\varepsilon > \frac{1}{4}$, see [6].

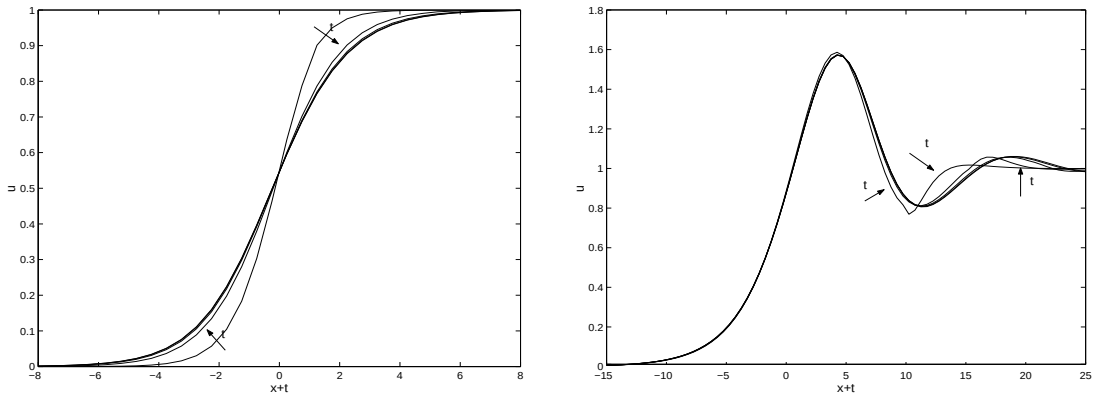

(a) $\varepsilon = 0.2$, $t = 5, 10, 15$ and 20.

(b) $\varepsilon = 5$, $t = 10, 15, 20, 25$ and 30.

Figure 2: Travelling wave type limiting profile.

4.3 Rarefaction waves

We take $u^- = 1$ and $u^+ = 0$ for simplicity, and as initial condition the step function

$$u_0(x) = \begin{cases} 0 & \text{if } x > 0 \\ 1 & \text{if } x \leq 0. \end{cases} \tag{4.8}$$

We expect the solution to approximate the rarefaction wave solution of the Burgers equation. We have taken the half length of the interval to be $l = 200$. The spatial step size is $h = 0.5$ and the temporal step size is $\tau = 0.01$. The solutions are shown in the rarefaction coordinate $\eta = x/2t$ at each time step. Figure 3 shows results for $\varepsilon = 0.2$ and $\varepsilon = 5$ at time steps $t = 10, 20, 30$ and 40. For both values of ε the profiles of the solution tend to overlap as t increases.

4.4 N-waves

In this section we consider examples for continuous compactly supported initial data. We namely take the following initial condition

$$u_0(x) = \begin{cases} \frac{-x}{25} & \text{if } -25 < x < 0 \\ \frac{x}{25} + 2 & \text{if } -50 \leq x < -25 \\ 0 & \text{otherwise.} \end{cases} \tag{4.9}$$

In this case we expect that the solution approximates a self-similar solution of the viscous Burgers' equation, which has the form $u(x,t) = \sqrt{t} f(x/\sqrt{t})$, and is a smooth approximation of solution of the inviscid equation, a so-called N-wave.

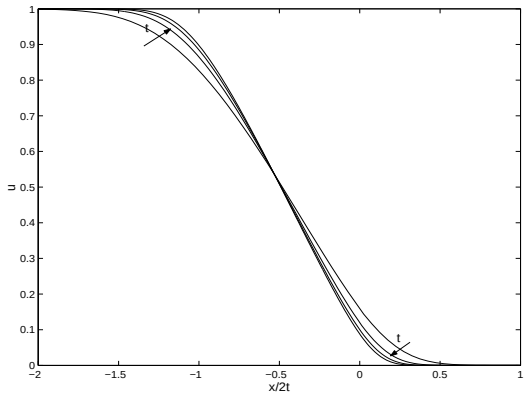

(a) $\varepsilon = 0.2$, $t = 10, 20, 30$ and 40.

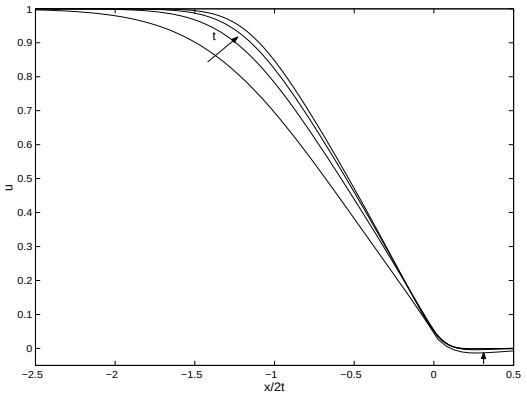

(b) $\varepsilon = 5$, $t = 10, 20, 30$ and 40.

Figure 3: Rarefaction wave type limiting profile.

We have taken the half length of the interval to be $l = 200$. The spatial step size is $h = 0.5$ and the temporal step size is $\tau = 0.1$. The solution is plotted in the self-similar variables: $x/\sqrt{t}$ against $u(x,t)\sqrt{t}$ for each time step. In Figure 4 the corresponding results for $\varepsilon = 0.2$ and $\varepsilon = 5$ are shown at time steps $t = 50, 100, 150, 200$ and 250.

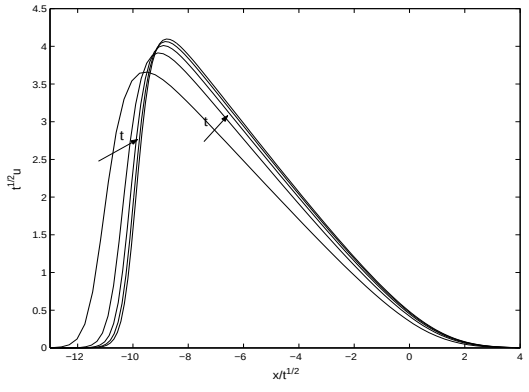

(a) $\varepsilon = 0.2$, $t = 50, 100, 150, 200$ and 250.

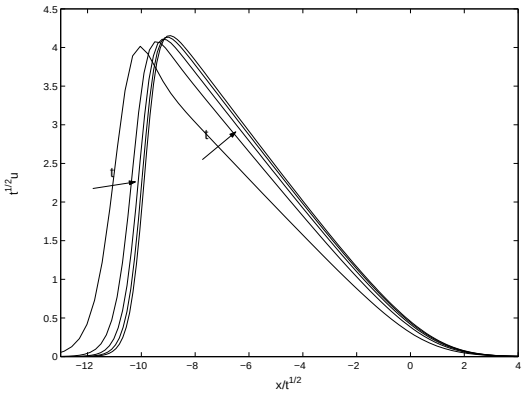

(b) $\varepsilon = 5$, $t = 50, 100, 150$ and 250.

Figure 4: N-wave type limiting profile.

4.5 Jump discontinuities

Figure 5 shows initial jump discontinuities decreasing with time. The initial data are respectively the Heaviside function, H, and its reverse, $1 - H$, as in (4.7) and (4.8). In both examples we have taken $\varepsilon = 5$, $\tau = 0.01$, $h = 0.5$ and $l = 200$. At the time steps $t = 4, 12$ and 20, the profile of the solution is shown against the spatial coordinate x.

In Figure 4.5, for small values of t the discontinuity and the oscillations of the solution generate a peak in the profile. This, however, disappears as t increases due to the decrease of the jump discontinuity.

In Figure 4.5, the solution becomes non-positive at early time steps. But the decrease on the jump, pushes up the solution as t increases. In particular the gives an example of non-positivity.

A Convergence results

In this section we give error estimates for both explicit and implicit discretization schemes. The initial data is assumed in H_0^1, and Homogeneous Dirichlet boundary conditions are taken. Results for less regular initial data can be obtained in similar fashion, leading eventually to lower convergence orders, but this lies beyond the purpose of this paper. Since we are working in one spatial dimension on a uniform grid, the spatial discretization described in Section 3 is equivalent to a first order mass lumping finite element formulation (see, e. g., [18]). In what follows we let $V_h \subset H_0^1(-l, l)$ denote the space of piecewise linear finite elements defined on the uniform grid with mesh size h.

The following inequalities will be used in the sequel, their proof being elementary.

$$\|u\|_\infty^2 \leq 2\|u\|\,\|u_x\| \leq \|u\|^2 + \|u_x\|^2 \leq \varepsilon^{-1/2}(\|u\|^2 + \varepsilon\|u_x\|^2) \tag{A.1}$$

$$\|u\|^2 \leq 4l\|u\|\,\|u_x\| \Rightarrow \|u\| \leq 4l\|u_x\| \tag{A.2}$$

A.1 Error estimates

We first consider only the spatial discretization of equation (1.3). This consists in seeking for $U \in C^1([0,T]; V_h)$ such that, for all $\chi \in V_h$ and all $t > 0$

$$(U_t, \chi) + \varepsilon(U_{xt}, \chi_x) = -(U_x, \chi_x) + ((U^2)_x, \chi). \tag{A.3}$$

The initial data is given by $(U(0), \chi) = (u_0, \chi)$ for all $\chi \in V_h$.

The following estimates hold.

Theorem A.1 *The semi-discrete solution U of problem (A.3) is defined for all $t \geq 0$, and satisfies the stability estimate*

$$\|U(t)\|_1 \leq C\|u_0\|_1 \tag{A.4}$$

for all $t > 0$, where $C = C_\varepsilon c_\varepsilon$ (the constants defined in (1.10)). The approximation error is bounded by

$$\|U(t) - u(t)\|_s \leq C(\|u_0\|_1)h^{1-s}\left(1 + \int_0^t (\|u_t(\nu)\|_1 + \|u(\nu)\|_1)d\nu\right) \tag{A.5}$$

for all $t > 0$ and $s = 0, 1$ respectively.

We refer to [2] for a proof given in a more general framework. The estimates are obtained for the standard finite element formulation. For stability reasons we have considered an mass lumped up-wind approach. Since both U and U_t are H^1 for any time, mass lumping does not affect the above results. However, up-winding may decrease the convergence order (see, e. g. [19] and [18]).

A.2 Explicit discretization

Applying a forward Euler discretization to equation (A.3) we look for $\{U^k\}_{k=\overline{1,m}} \subset V_h$ such that

$$\left(U^k - U^{k-1}, \chi\right) + \varepsilon \left(U_x^k - U_x^{k-1}, \chi_x\right) = -\tau(U_x^{k-1}, \chi) - \tau((U^{k-1})^2, \chi_x) \tag{A.6}$$

for all $\chi \in V_h$, with $U^0 = U(0) \in V_h$. The following estimates are proved in [2].

Theorem A.2 *Let U^k and u solving (A.6), respectively (1.3), then the approximation error is bounded by*

$$\|u(t_k) - U^k\|_s \leq h^{1-s} C_1 + \tau C_2 \int_0^{t_k} \|U_{tt}(\nu)\|_1 \, d\nu \tag{A.7}$$

where

$$C_1 = C(\|u_0\|_1) \left(1 + \int_0^1 (\|u_t(\nu)\|_1 + \|u(\nu)\|_1) d\nu\right),$$

and C_2 is a positive constant that depends on the uniform bound of the solutions on $[0, T]$ and on T.

A.3 Implicit discretization

The implicit scheme can be defined in a similar manner. We seek for $\{U^k\}_{k=\overline{1,m}} \subset V_h$ such that, for all $\chi \in V_h$,

$$(U^k - U^{k-1}, \chi) + \varepsilon(U_x^k - U_x^{k-1}, \chi_x) = -\tau(U_x^k, \chi_x) - \tau((U^k)^2, \chi_x). \tag{A.8}$$

Testing (A.8) with $\chi = U^k$ and using (A.9) and (A.1) we readily get the following *a priori* estimates.

Lemma A.3 *Let U^k be a solution of (A.8), then*

$$\|U^k\|_\varepsilon \leq \|U^{k-1}\|_\varepsilon \tag{A.9}$$

for $k = 1, \ldots, m$. In particular

$$\|U^k\|_\infty \leq \frac{1}{\varepsilon^{1/4}} \|u_0\|_\varepsilon \tag{A.10}$$

for all m.

Analogous to Theorem A.2 we have the following theorem

Theorem A.4 *Let U^{k+1} and u solving (A.8) and (1.3) respectively, then*

$$\|u(t_k) - U^k\|_s \leq h^{1-s} C_1 + \tau C_2 \int_0^{t_k} \|U_{tt}\|_1 \, d\nu \tag{A.11}$$

where

$$C_1 = C(\|u_0\|_1) \left(1 + \int_0^1 (\|u_t(\nu)\|_1 + \|u(\nu)\|_1) d\nu\right),$$

and C_2 is a positive constant that depends on T and $\|u_0\|_1$.

The error estimates for (A.8) are obtained in the same fashion as for the explicit scheme. Details are omitted here.

A.4 Iterative process

This section is dedicated to prove convergence of the iteration procedure given by (3.9) in the FEM framework, so we assume that the boundary conditions are homogeneous and $u^0 \in H_0^1(-l,l)$.

We use the following notation

$$M_U := \|U^0\|_\varepsilon^2,$$

then by Lemma A.3 and (A.1) we have

$$\|U^k\|_\infty^2 \le \varepsilon^{-1/2} M_U \quad \text{for any } k \ge 0. \tag{A.12}$$

. Now the iterative procedure can be written as follows. Fix $k > 0$ and let U^{k-1} solve (A.8). For any $s > 0$ find $U^{k,s} \in H_0^1(-l,l)$ such that for all $\chi \in H_0^1(-l,l)$ we have

$$(U^{k,s},\chi) + (\varepsilon+\tau)(U_x^{k,s},\chi_x) + \tau(U^{k,s-1}U^{k,s},\chi_x) = (U^{k-1},\chi) + \varepsilon(U_x^{k-1},\chi_x), \tag{A.13}$$

with $U^{k,0} = U^{k-1}$.

For each s, existence and uniqueness of a solution is provided by standard arguments (monotone perturbation of bounded and coercive bilinear forms). Moreover, the resulting array can be bounded *a priori*.

Lemma A.5 *Denote by $\alpha = 16l^2/(16l^2+\varepsilon) \in (0,1)$ and assume τ satisfying*

$$\tau \le \frac{\alpha\varepsilon^{3/2}}{8l^2 M_U} = \frac{2\varepsilon^{3/2}}{M_U(16l^2+\varepsilon)}. \tag{A.14}$$

If U^{k-1} solves (A.8), then for each $i \ge 0$ the solution of (A.13) satisfies

$$\|U^{k,s}\|^2 + \varepsilon\|U_x^{k,s}\|^2 \le M_U \frac{(1-\alpha^{s+1})}{1-\alpha}. \tag{A.15}$$

Proof. The proof will be done by mathematical induction. For $U^{k,0} = U^{k-1}$ (A.15) obviously holds. Fix now $s > 0$ and assume (A.15) for $U^{k,s-1}$. Denoting by M_s the H^1 equivalent norm of $U^{k,s}$

$$M_s := \|U^{k,s}\|^2 + \varepsilon\|U_x^{k,s}\|^2,$$

by (A.1) we have

$$\|U^{k,s-1}\|_\infty^2 \le \varepsilon^{-1/2} M_{s-1}. \tag{A.16}$$

Taking $\chi = U^{k,s}$ into (A.13) and using Cauchy's inequality yields

$$\begin{aligned}\|U^{k,s}\|^2 + (\varepsilon+\tau)\|U_x^{k,s}\|^2 \le\ & \tau\varepsilon^{-1/4} M_{s-1}^{1/2}\|U^{k,s}\|\|U_x^{k,s}\| \\ & + \|U^{k-1}\|\,\|U^{k,s}\| + \varepsilon\|U_x^{k-1}\|\,\|U_x^{k,s}\|.\end{aligned}$$

Applying the mean inequality $2|ab| \le \nu|a|^2 + |b|^2/\nu$ for any reals a, b and $\nu > 0$ (with $\nu_1 = \varepsilon^{-1/4} M_{s-1}^{1/2}/2$, $\nu_2 = 1$ and $\nu_3 = 1$), after multiplying by 2 we end up with

$$\begin{aligned}2\|U^{k,s}\|^2 + 2(\varepsilon+\tau)\|U_x^{k,s}\|^2 \le\ & \tfrac{\tau\varepsilon^{-1/2}M_{s-1}}{2}\|U^{k,s}\|^2 + 2\tau\|U_x^{k,s}\|^2 \\ & + \|U^{k-1}\|^2 + \|U^{k,s}\|^2 + \varepsilon\|U_x^{k-1}\|^2 + \varepsilon\|U_x^{k,s}\|^2.\end{aligned}$$

This can be rewritten as

$$\left(1 - \tfrac{\tau\varepsilon^{-1/2}M_{s-1}}{2}\right)\|U^{k,s}\|^2 + \varepsilon\|U_x^{k,s}\|^2 \leq \|U^{k-1}\|^2 + \varepsilon\|U_x^{k-1}\|^2. \tag{A.17}$$

The choice of α and (A.14) ensures that the factor multiplying $\|U^{k,s}\|^2$ above is positive. Therefore Lemma A.3 gives

$$\varepsilon\|U_x^{k,s}\|^2 \leq M_U,$$

which, together with (A.2) leads to

$$\|U^{k,s}\|^2 \leq 16l^2 M_U/\varepsilon.$$

Applying the last inequality into (A.17) and gets

$$M_s = \|U^{k,s}\|^2 + \varepsilon\|U_x^{k,s}\|^2 \leq M_U\left(1 + \tau 8l^2\varepsilon^{-3/2}M_{s-1}\right), \tag{A.18}$$

which, together with (A.14) proves the induction assumption. □

Remark A.6 *The lemma above guarantees that, under the given restrictions on τ, the iteration array $\{U^{k,s}\}_{s\geq 0}$ is bounded in H^1. In fact, by (A.1), for all $s \geq 0$ we have*

$$\|U^{k,s}\|^2 + \varepsilon\|U_x^{k,s}\|^2 \leq \frac{M_U}{1-\alpha}, \quad \text{and} \quad \|U^{k,s}\|_\infty \leq \frac{M_U}{\sqrt{\varepsilon}(1-\alpha)}.$$

In this way we have shown that the iteration array is uniformly bounded in both H^1 and L^∞. We will use this result for proving that the iteration (A.13) converges to U^k.

Theorem A.7 *Let $k > 0$ be fixed and assume τ satisfying both (A.14) and*

$$\tau < \frac{\sqrt{2}\varepsilon^2}{M_U[\varepsilon^2 + (16l^2+\varepsilon)^2]^{1/2}}. \tag{A.19}$$

Then the iteration array $\{U^{k,s}\}_{s\geq 0}$ defined by (A.13) converges to the solution U^k of (A.8) strongly in H^1.

Remark A.8 *Note that the conditions (A.14) and (A.19) do not depend on k or s.*

Proof. In what follows we denote the error at the iteration i by $e^s := U^k - U^{k,s}$. Subtracting (A.13) from (A.8) gives

$$(e^s, \chi) + (\varepsilon+\tau)(e_x^s, \chi_x) + \tau(U^k e^s + U^{k,s}e^{s-1}, \chi_x) = 0. \tag{A.20}$$

Taking into above $\chi = e^s$, Cauchy's inequality gives

$$\|e^s\|^2 + (\varepsilon+\tau)\|e_x^s\|^2 \leq \tau\varepsilon^{-1/2}M_U\|e^s\|\,\|e_x^s\| + \tau\varepsilon^{-3/2}M_U(16l^2+\varepsilon)\|e^{s-1}\|\,\|e_x^s\|,$$

where we have also used Lemma A.3 and Remark A.6. Using now the mean inequality yields

$$\begin{aligned}\|e^s\|^2 + (\tau+\varepsilon)\|e_x^s\|^2 \leq{}& \frac{\tau M_U}{2\varepsilon^{\frac{1}{4}}}\left(\delta_1\|e^s\|^2 + \frac{1}{\delta_1}\|e_x^s\|^2\right)\\ &+\frac{\tau M_U}{2\varepsilon^{\frac{1}{2}}(16l^2+\varepsilon)}\left(\delta_2\|e^{s-1}\|^2 + \frac{1}{\delta_2}\|e_x^s\|^2\right).\end{aligned}$$

We choose $\delta_1 = \frac{\tau M_U}{\varepsilon^{\frac{3}{2}}}$ and $\delta_2 = \frac{M_U(16l^2+\varepsilon)\tau}{\varepsilon^{\frac{5}{2}}}$, then

$$\left(1 - \frac{\tau^2 M_U^2}{2\varepsilon^2}\right)\|e^s\|^2 + \tau\|e_x^s\|^2 \leq \frac{\tau^2 M_U^2(16l^2+\varepsilon)^2}{2\varepsilon^4}\|e^{s-1}\|^2. \tag{A.21}$$

Since τ satisfies (A.19) it follows that

$$\left(1 - \frac{\tau^2 M_U^2}{2\varepsilon^2}\right) > \frac{\tau^2 M_U^2(16l^2+\varepsilon)^2}{2\varepsilon^4} > 0, \tag{A.22}$$

and hence

$$\|e^s\|^2 + \frac{2\tau\varepsilon^2}{2\varepsilon^2 - \tau^2 M_U^2}\|e_x^s\|^2 \leq \frac{\tau^2 M_U^2(16l^2+\varepsilon)^2}{\varepsilon^2(2\varepsilon^2 - \tau^2 M_U^2)}\left(\|e^{s-1}\|^2 + \frac{2\tau\varepsilon^2}{2\varepsilon^2 - \tau^2 M_U^2}\|e_x^{s-1}\|^2\right).$$

By (A.22), the multiplication factor on the right is less than 1, which immediately implies that $e^s \to 0$ strongly in H^1. □

Acknowledgements: The authors acknowledge J. Hulshof and J.R. King for useful comments. Also I.S.P. acknowledges the financial support provided by the Dutch government through the BSIK program, project BRICKS, theme MSV1.

References

[1] C. Amick, J. Bona, and M. Schonbek. Decay of solutions of some nonlinear wave equations. *J. Differential Equations*, 81:1–19, 1989.

[2] D. N. Arnold, J. J. Douglas, and V. Thomée. Superconvergence of a finite element approximation to the solution of a Sobolev equation in a single space variable. *Math. Comp.*, 36:53–63, 1981.

[3] J. Bear. *Dynamics of fluids in porous media*. Elsevier, New York, 1972.

[4] J. Bear and Y. Bachmat. *Introduction to modelling of transport phenomenoa in porous media*. Kluwer, Dordrecht, 1991.

[5] T. B. Benjamin, J. L. Bona, and J. J. Mahony. Model equations for long waves in nonlinear dispersive systems. *Philos. Trans. Roy. Soc. London Ser. A*, 272:47–78, 1972.

[6] C. Cuesta and J. Hulshof. A model problem for groundwater flow with dynamic capillary pressure: stability of travelling waves. *Nonlinear Anal.*, 52:1199–1218, 2003.

[7] C. Cuesta, C. J. van Duijn, and J. Hulshof. Infiltration in porous media with dynamic capillary pressure: travelling waves. *European J. Appl. Math.*, 11:381–397, 2000.

[8] C. M. Cuesta. *Pseudo-parabolic equations with driving convection term*. PhD thesis, Vrije Universiteit Amsterdam, 2003.

[9] R. E. Ewing. Time-stepping Galerkin methods for nonlinear Sobolev partial differential equations. *SIAM J. Numer. Anal.*, 15:1125–1150, 1978.

[10] S. M. Hassanizadeh and W. G. Gray. Thermodynamic basis of capillary pressure in porous media. *Water Resour. Res.*, 29:3389–3405, 1993.

[11] S. M. Hassanizadeh, R. J. Schotting, and A. Y. Beliaev. A new capillary pressure-saturation relationship including hysteresis and dynamic effects. In B. et.al, editor, *Proceedings of the XIII International Conference on Computational Methods in Water Resources*, pages 245–251, Calgary, Canada, June 2000. Balkema.

[12] R. Helmig, A. Weiss, and B. Wohlmuth. Dynamic capillary effects in heterogeneous media. Submitted.

[13] E. Hopf. The partial differential equation $u_t + uu_x = \mu u_{xx}$. *Comm. Pure Appl. Math.*, 3:201–230, 1950.

[14] A. M. Il′in and O. A. Oleĭnik. Asymptotic behavior of solutions of the Cauchy problem for some quasi-linear equations for large values of the time. *Mat. Sb. (N.S.)* English transl. in *Amer. Math. Soc. Translations.*, pages 19–23, 1964.

[15] P. G. LeFloch. *Hyperbolic systems of conservation laws*. Lectures in Mathematics ETH Zürich. Birkhäuser Verlag, Basel, 2002. The theory of classical and nonclassical shock waves.

[16] R. J. LeVeque. *Numerical methods for conservation laws*. Birkhäuser Verlag, Basel, second edition, 1992.

[17] T. P. Liu. Invariants and asymptotic behavior of solutions of a conservation law. *Proc. Amer. Math. Soc.*, 71:227–231, 1978.

[18] A. Quarteroni and A. Valli. *Numerical approximation of partial differential equations*. Springer-Verlag, Berlin, 1994.

[19] V. Thomée. *Galerkin finite element methods for parabolic problems*. Springer-Verlag, Berlin, 1984.

[20] C. van Duijn, J. Molenaar, and M. de Neef. The effect of capillary forces on immisble two-phase flow in heterogeneous porous media. *Transp. Porous Media*, 21:71–93, 1995.

[21] C. van Duijn, L. Peletier, and I. Pop. A new class of entropy solutions of the Buckley-Leverett equation. to appear in SIAM J. Math Anal.

[22] C. J. van Duijn, A. Mikelič, and I. S. Pop. Effective equations for two-phase flow with trapping on the micro scale. *SIAM J. Appl. Math.*, 62:1531–1568, 2002.

[23] J. L. Vázquez and E. Zuazua. Complexity of large time behaviour of evolution equations with bounded data. In *Frontiers in mathematical analysis and numerical methods*, pages 267–295. World Sci. Publ., River Edge, NJ, 2004.

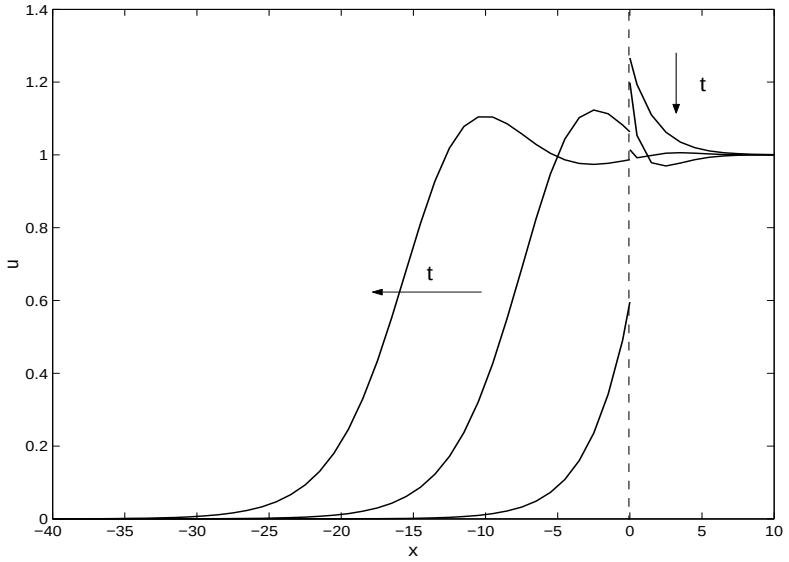

(a) $\varepsilon = 5$, $t = 4, 12$ and 20.

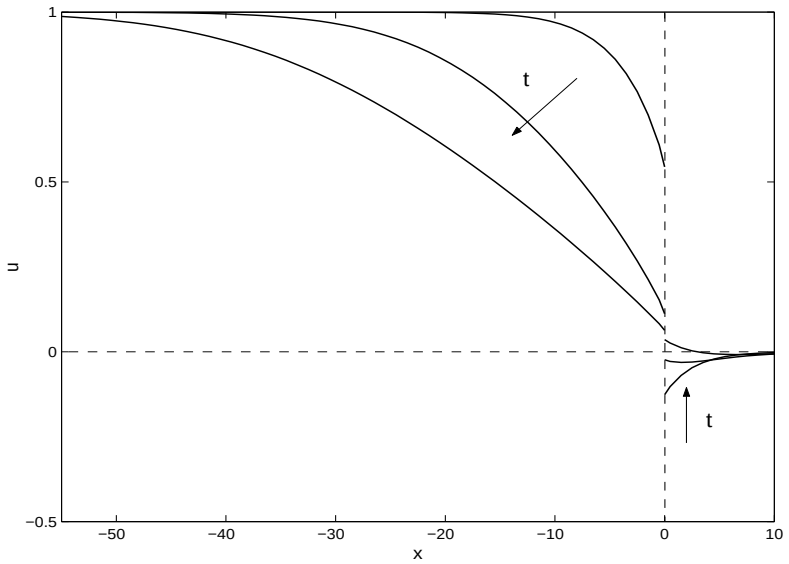

(b) $\varepsilon = 5$, $t = 4, 12$ and 20.

Figure 5: Persistence of discontinuities in x.